Meteoritics & Planetary Science 36, 107–122 (2001)
Available online at http://www.uark.edu/meteor

The Monahans chondrite and halite: Argon-39/argon-40 age, solar gases, cosmic-ray exposure ages, and parent body regolith neutron flux and thickness

DONALD D. BOGARD[1]*, DANIEL H. GARRISON[1,2] AND JOZEF MASARIK[3]

[1]Planetary Sciences, Mail Code SN2, Johnson Space Center, Houston, Texas 77058, USA
[2]Lockheed-Martin Corporation, Houston, Texas 77058, USA
[3]Nuclear Physics Department, Komensky University, Bratislava, Slovakia
*Correspondence author's e-mail address: donald.d.bogard@jsc.nasa.gov

(Received 2000 May 25; accepted in revised form 2000 September 29)

Abstract–The Monahans H-chondrite is a regolith breccia containing light and dark phases and the first reported presence of small grains of halite. We made detailed noble gas analyses of each of these phases. The ^{39}Ar-^{40}Ar age of Monahans light is 4.533 ± 0.006 Ma. Monahans dark and halite samples show greater amounts of diffusive loss of ^{40}Ar and the maximum ages are 4.50 and 4.33 Ga, respectively. Monahans dark phase contains significant concentrations of He, Ne and Ar implanted by the solar wind when this material was extant in a parent body regolith. Monahans light contains no solar gases. From the cosmogenic ^{3}He, ^{21}Ne, and ^{38}Ar in Monahans light we calculate a probable cosmic-ray, space exposure age of 6.0 ± 0.5 Ma. Monahans dark contains twice as much cosmogenic ^{21}Ne and ^{38}Ar as does the light and indicates early near-surface exposure of 13–18 Ma in a H-chondrite regolith. The existence of fragile halite grains in H-chondrites suggests that this regolith irradiation occurred very early. Large concentrations of ^{36}Ar in the halite were produced during regolith exposure by neutron capture on ^{35}Cl, followed by decay to ^{36}Ar. The thermal neutron fluence seen by the halite was (2–4) × 10^{14} n/cm^2. The thermal neutron flux during regolith exposure was ~0.4–0.7 n/cm^2/s. The Monahans neutron fluence is more than an order of magnitude less than that acquired during space exposure of several large meteorites and of lunar soils, but the neutron flux is lower by a factor of ≤5. Comparison of the $^{36}Ar_n/^{21}Ne_{cos}$ ratio in Monahans halite and silicate with the theoretically calculated ratio as a function of shielding depth in an H-chondrite regolith suggests that irradiation of Monahans dark occurred under low shielding in a regolith that may have been relatively shallow. Late addition of halite to the regolith can be ruled out. However, irradiation of halite and silicate for different times at different depths in an extensive regolith cannot be excluded.

INTRODUCTION

In the recently fallen Monahans, Texas H-5 chondrite, Zolensky *et al.* (1999a) report the occurrence of mm-size grains of halite (NaCl), which contain microscopic inclusions of water-brine and minor amounts of sylvite (KCl). This is the first reported occurrence of brine-containing halite inclusions in meteorites, and their presence is inferred to have important implications for the occurrence of liquid water on chondrite parent bodies (Zolensky *et al.*, 1999a). Subsequently, similar halite inclusions were reported in the Zag H-chondrite (Zolensky *et al.*, 1999b). The halite readily dissolves in a humid environment, and halite thus may be relatively common in chondrite falls, but has gone undetected until now. Monahans and Zag also contain abundant light silicate clasts set in a darker silicate matrix, and the dark phase is the host for the halite. Monahans also contains a few small black clasts set in the same dark matrix. We show in this paper that the dark matrix of Monahans also contains implanted solar noble gases, which prove its prior existence in a regolith at the H-chondrite parent body surface. Because the halite is a part of this regolith, the origin and mode of formation of the halite is somewhat obscured. Zolensky *et al.* (1999a) suggested two possible origins for the halite: dissolution and precipitation by water flowing within the parent asteroid, or delivery to the asteroid regolith surface from an outside source such as a salt-containing icy object.

We have measured various noble gas components in Monahans silicate and halite to further characterize the environment and history of this meteorite. In addition to finding solar gases in the dark phase, we also determined ^{39}Ar-^{40}Ar ages of the silicate and the halite and the cosmic-ray exposure ages of the light phase during space exposure and of the dark phase during prior regolith exposure. Preliminary data were reported in Zolensky *et al.* (1999c). Further, the high Cl content of the halite enables determination of the neutron fluence in

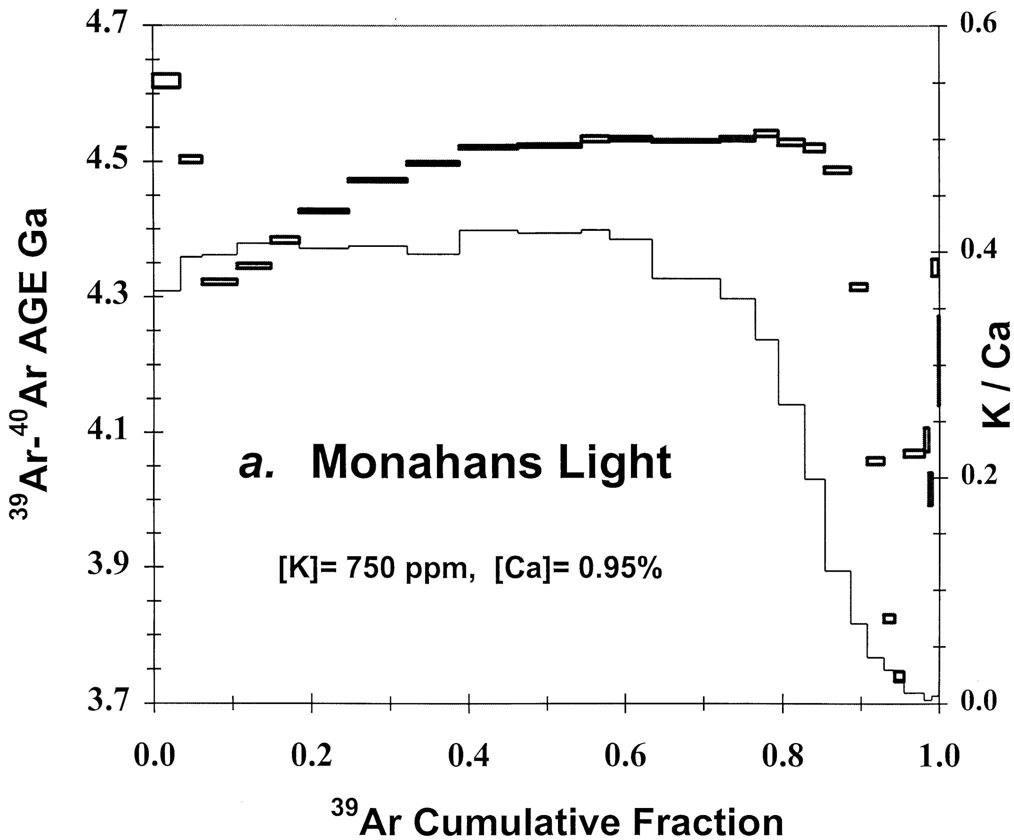

FIG. 1. ^{39}Ar-^{40}Ar age (rectangles; left scale) and K-Ca ratio (stepped line; right scale) as a function of cumulative ^{39}Ar release for stepwise temperature extractions of (a) Monahans light, (b) Monahans dark regolith *(facing page, top)*, and (c) Monahans halite *(facing page, bottom)*. The analytical uncertainty in each age is indicated by the width of the rectangle. Determined K and Ca concentrations are indicated.

the parent body regolith. When this fluence is combined with theoretical models of formation rates of nuclear reaction products as a function of shielding some constraints can be placed on the nature of the Monahans regolith irradiation.

SAMPLES AND TECHNIQUES

We obtained from C. B. Moore and E. K. Gibson three samples of Monahans silicate: dark phase, light clast material, and part of a small black inclusion or clast within the dark phase. From M. Zolensky we obtained a 1.87 mg sample of Monahans halite, plucked from the dark phase. All of the halite and samples of the light and dark (regolith) silicate phases were neutron-irradiated for ^{39}Ar-^{40}Ar dating. Six samples of the hornblende NL-25 age monitor irradiated with Monahans reveal a slight gradient in neutron flux across the samples and define neutron irradiation constants (*J* values) of 0.03073 ± 0.00006 (light), 0.03066 ± 0.00006 (dark), and 0.03086 ± 0.00006 (halite). Ar was extracted by stepwise degassing and its isotopic composition was measured on a Nuclide 6-60 mass spectrometer. Corrections to the Ar isotopic data were applied for system blanks, radioactive decay, and reactor-produced interferences. Detailed explanations of the analytical and age calculation techniques, the NL-25 age standard used, the reactor corrections applied, and the use of irradiations constants are given in Bogard *et al.* (1995a, 2000). Separate samples of unirradiated Monahans silicate were degassed in stepwise temperature release for the purpose of measuring cosmogenic and trapped noble gas concentrations. These were measured on a VG-3600 mass spectrometer that has not seen gas from irradiated samples.

RESULTS

^{39}Ar-^{40}Ar Ages

Ar isotopic data, K/Ca ratios, and calculated ages for three irradiated Monahans samples are given in Appendix 1. The ^{39}Ar-^{40}Ar age spectra and K/Ca ratios as a function of cumulative release of ^{39}Ar are shown in Fig. 1. Age uncertainties for individual extractions shown in the figures represent only the analytical uncertainties in determining ^{40}Ar/^{39}Ar ratios (Bogard *et al.*, 2000).

Although the Monahans light and dark silicate samples show complex age spectra, we believe that their interpretation is straightforward. For Monahans light the K/Ca ratios are relatively constant at ~0.4 over ~0–80% of the ^{39}Ar release and represent degassing of feldspar. Above ~80% ^{39}Ar release,

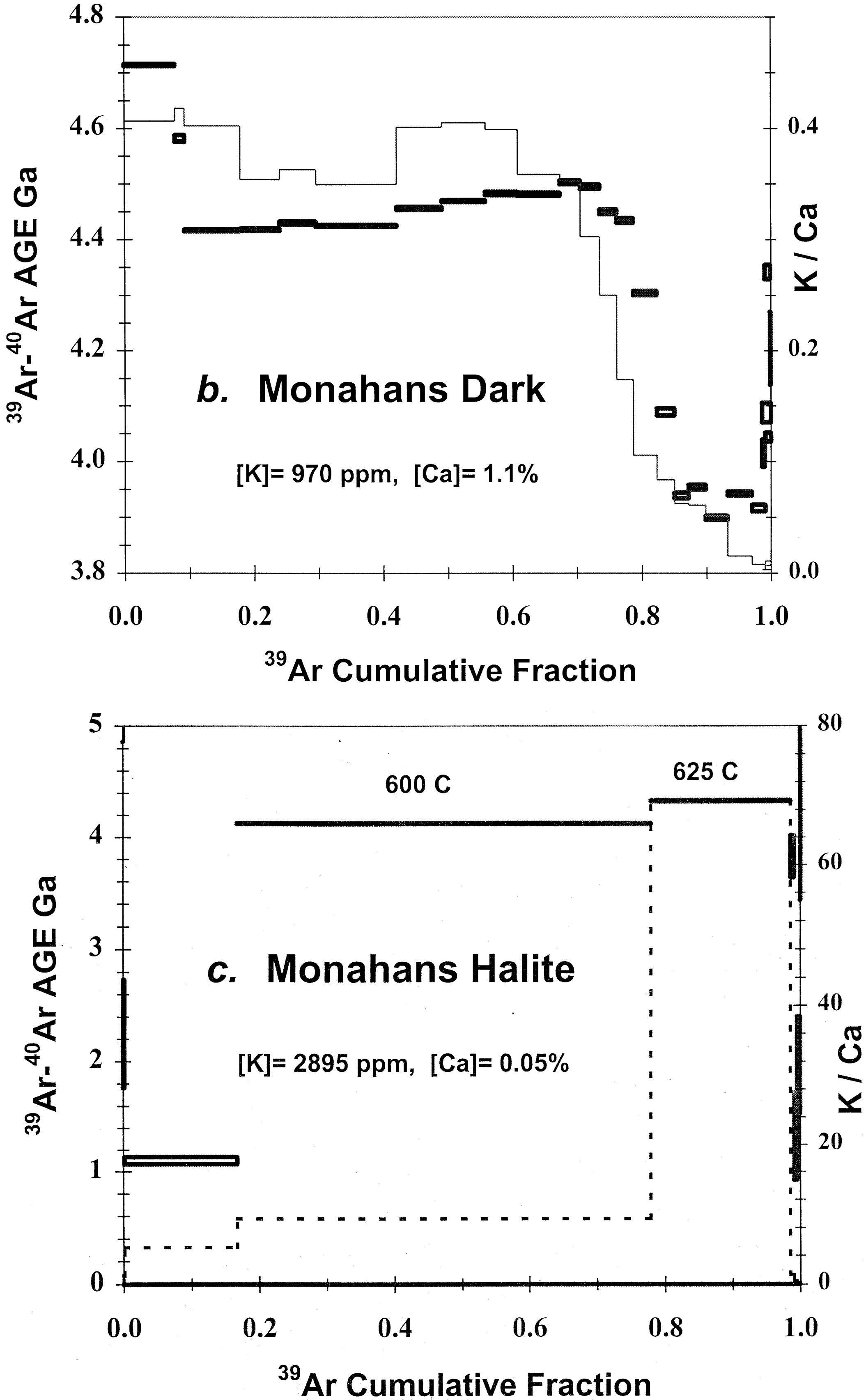
4.8
4.6
4.4
4.2
4.0
3.8
0.4
0.2
0.0
^{39}Ar-^{40}Ar AGE Ga
K / Ca
b. Monahans Dark
[K]= 970 ppm, [Ca]= 1.1%
0.0
0.2
0.4
0.6
0.8
1.0
^{39}Ar Cumulative Fraction
5
4
3
2
1
0
80
60
40
20
0
600 C
625 C
c. Monahans Halite
[K]= 2895 ppm, [Ca]= 0.05%
^{39}Ar-^{40}Ar AGE Ga
K / Ca
0.0
0.2
0.4
0.6
0.8
1.0
^{39}Ar Cumulative Fraction

the K/Ca ratios decrease dramatically and represent additional Ar degassing from pyroxene. We attribute the significant decrease in Ar-Ar age above ~80% ^{39}Ar release to capture of recoiled ^{39}Ar onto grain surfaces of these mafic minerals. Recoil transfer of ^{39}Ar between mineral phases of fine-grained samples occurs in the formation of ^{39}Ar during neutron irradiation and is commonly observed in irradiated meteorites. This captured ^{39}Ar, which is released at higher extraction temperatures because of its location in pyroxene, causes a decrease in the ^{40}Ar/^{39}Ar ratio and thus the age for these extractions. Lowering of the Ar-Ar ages by ^{39}Ar recoil is greater at ~95% ^{39}Ar release of Monahans light compared to higher temperature releases because this represents degassing of surfaces of mafic grains where the recoiled ^{39}Ar is deposited. (The recoil distance of ^{39}Ar in silicate is <0.2 μm.) The source of this recoiled ^{39}Ar was from surfaces of feldspar grains, which released Ar at low temperatures. Consequently, the Ar-Ar ages of low-temperature extractions should be artificially elevated. The first few extractions (~0–7% ^{39}Ar release) do show elevated Ar-Ar ages relative to subsequent extractions. (Corrections for terrestrial Ar based on trapped ^{36}Ar does not significant lower the apparent ages for these first two extractions.) However, the extent to which ages of low temperature extractions have been elevated by ^{39}Ar recoil cannot be accurately estimated because the surfaces of feldspar grains in Monahans light have apparently lost some ^{40}Ar by diffusion. This loss is evident in the monotonic increase in Ar-Ar ages for extractions between ~7% and ~39% of the ^{39}Ar release and is also a phenomenon commonly seen in meteorites. To a first approximation, the amount of ^{39}Ar recoil loss from feldspar grain surfaces degassing at low temperatures appears to be equivalent to ^{39}Ar gain by surfaces of mafic grains degassing at high temperatures.

The Ar-Ar age spectrum for the Monahans dark matrix sample (Fig. 1b) can be similarly interpreted. For the dark sample, however, the ^{39}Ar gained by high-temperature mafic phases is somewhat greater than for the light sample and seems to be greater than the apparent recoil loss of ^{39}Ar at lower extraction temperatures (evident in elevated Ar-Ar ages). However, Monahans dark appears not to have lost as much ^{40}Ar by diffusion as has Monahans light, even though the dark matrix may have a smaller average grain size. We suspect that the dark phase actually did lose significant ^{40}Ar by diffusion and this fact is masked by relatively large elevation of the Ar-Ar age over 0–40% ^{39}Ar release because of ^{39}Ar recoil.

Most probably the interiors of feldspar grains in both Monahans silicate samples did not participate in the exchange of recoiled ^{39}Ar between mineral phases. Thus, the ages at intermediate extraction temperatures should yield the most accurate Ar-Ar ages. For the Monahans light sample, nine extractions releasing over ~38–85% of the total ^{39}Ar give a ^{39}Ar-^{40}Ar age of 4.529 ± 0.008 Ga (Fig. 1a). Six extractions releasing over ~54–82% of the total ^{39}Ar give an age of 4.533 ± 0.007 Ga. The total age summed over all extractions is 4.44 Ga. Uncertainties in these "plateau" ages are statistically calculated from variations among ages of individual extractions and the uncertainty in J (Bogard *et al.*, 2000). For the Monahans dark regolith sample, 10 extractions releasing over ~9–73% of the total ^{39}Ar give an age of 4.449 ± 0.034 Ga (Fig. 1b). However, these extractions show a sloped age spectrum, suggesting diffusive loss of ^{40}Ar (see comment above). The two extractions at ~70% ^{39}Ar release give the highest age observed of ~4.50 Ga. The total age for Monahans dark summed over all extractions is 4.38 Ga. The lower apparent Ar-Ar ages and greater effects of ^{39}Ar recoil at higher release temperatures for the Monahans dark regolith sample compared to the light sample suggests that comminution on the parent body surface caused some reduction in average grain size of regolith material and may have produced some diffusive loss of ^{40}Ar.

The sample of Monahans halite (Fig. 1c) released 98.4% of its ^{39}Ar in three extractions over 500–625 °C. The determined K concentration of 0.29% indicates that sylvite (KCl) was a relatively minor phase within the NaCl. The Ar-Ar age spectrum indicates significant prior diffusive loss of ^{40}Ar. We consider the maximum measured age of 4.33 ± 0.01 Ga in the 625 °C extraction to represent a minimum formation age of the halite. Extractions above 625 °C (including one at 650 °C) released Ar amounts that were only slightly above blank levels. (NaCl melts at 801 °C, and KCl at ~770 °C.) This highest Ar-Ar age is lower than a Rb-Sr model age of 4.7 ± 0.2 Ga obtained from a single analysis of Monahans halite (Zolensky *et al.*, 1999a).

We conclude that the Ar-Ar age of ~4.53 Ga for the Monahans host represents the time when post-metamorphism cooling after formation of the Monahans parent body had reached temperatures of no more than a few hundred Celsius. This Ar-Ar age ranks among the oldest such ages for meteorites. For example, Turner *et al.* (1978) reported Ar-Ar ages of 4.44–4.52 Ga for several unshocked ordinary chondrites. The slightly younger Ar-Ar ages for the dark phase and the halite probably represent greater amounts of ^{40}Ar diffusion loss during grain residence in a parent body regolith. For Zag, the second H-chondrite with recognized halite inclusions, Whitby *et al.* (2000) reported Ar-Ar ages of 4.29 and 4.25 Ga for light and dark silicate phases, respectively, and 4.03 and 4.66 Ga for two halite samples. These authors also report an old I-Xe age of Zag halite (relative to most meteorites), indicating very early halite formation. Formation of the halite in both Monahans and Zag may have occurred as a result of water mobilization during early parent body metamorphism, whereas the Ar-Ar ages of silicate probably represent cooling after metamorphism.

Trapped Solar Gases

Concentrations of noble gases measured in stepwise temperature extractions of three non-irradiated silicate samples

TABLE 1. Measured concentrations (cm^3 STP/g in units indicated) of noble gases in stepwise temperature extractions of three samples of Monahans.

Sample Temp. (°C)	^{3}He (10^{-8})	^{4}He (10^{-6})	^{22}Ne (10^{-8})	^{36}Ar (10^{-8})	^{40}Ar (10^{-5})	^{20}Ne/^{22}Ne	^{21}Ne/^{22}Ne	^{36}Ar/^{38}Ar	^{84}Kr (10^{-10})	^{132}Xe (10^{-10})	^{129}Xe (10^{-10})
Light											
500	3.64	11.24	0.08	0.05	0.17	1.400 ± 0.038	0.821 ± 0.004	2.169 ± 0.044	n.m.	n.m.	n.m.
1600	5.55	9.91	2	0.67	3.94	0.878 ± 0.002	0.932 ± 0.002	1.873 ± 0.005	n.m.	1.21	1.54
Total	9.19	21.15	2.08	0.72	4.11	0.899 ± 0.003	0.928 ± 0.002	1.892 ± 0.006	–	–	–
Dark											
450	6.97	138	3.17	0.78	1.61	13.386 ± 0.035	0.0598 ± 0.0002	5.026 ± 0.013	n.m.	n.m.	n.m.
525	2.38	48.4	1.69	0.39	0.82	12.978 ± 0.006	0.0591 ± 0.0005	4.706 ± 0.022	n.m.	n.m.	n.m.
650	4.7	99.5	4.44	2.86	1.48	12.692 ± 0.009	0.0650 ± 0.0001	5.225 ± 0.005	n.m.	n.m.	n.m.
750	3.33	51.6	1.91	4.29	0.71	10.951 ± 0.006	0.1458 ± 0.0002	5.278 ± 0.003	n.m.	n.m.	n.m.
850	1.53	20.3	2.21	1.08	0.31	10.132 ± 0.002	0.1920 ± 0.0001	5.038 ± 0.010	n.m.	0.06	0.15
1050	2.35	13.2	9.08	2.81	0.44	10.350 ± 0.016	0.1603 ± 0.0002	4.480 ± 0.007	n.m.	0.37	0.63
1300	1.01	4.9	3.4	3.37	0.3	6.635 ± 0.004	0.4330 ± 0.0004	3.910 ± 0.003	n.m.	1.48	1.80
1600	0.006	0.08	0.24	0.31	0.02	2.612 ± 0.013	0.7800 ± 0.0020	3.562 ± 0.020	n.m.	0.37	0.47
Total	22.28	376	26.1	15.84	5.67	10.757 ± 0.004	0.1681 ± 0.0001	4.689 ± 0.002	n.m.	2.29	3.05
Clast											
300	0.54	4.7	0.09	0.19	0.21	10.829 ± 0.09	0.1329 ± 0.0069	5.441 ± 0.146	n.m.	n.m.	n.m.
650	5.58	57	3.79	1.35	5.67	12.382 ± 0.015	0.0921 ± 0.0004	4.831 ± 0.039	n.m.	0.27	0.35
1600	5.82	27.7	7.25	5.46	4.37	8.154 ± 0.010	0.3425 ± 0.0004	4.305 ± 0.007	1.41	3.49	5.09
Total	11.95	89.5	11.1	6.99	10.25	9.616 ± 0.008	0.2555 ± 0.0003	4.422 ± 0.009	–	3.76	5.44

n.m. = not measured.

of Monahans are given in Table 1. Kr and Xe released from meteorites at low temperature is frequently dominated by adsorbed terrestrial gases. Thus, Xe was not measured in the first temperature extraction. Kr was not measured in any extraction of the light and dark samples, but was measured in the dark clast. Figure 2 compares abundances of trapped ^{4}He, ^{20}Ne, ^{36}Ar, ^{84}Kr (clast only), and ^{132}Xe in Monahans samples with these abundances in the Pesyanoe aubrite (Marti, 1969) and in C1 and CM chondrites (Mazor *et al.*, 1970). Pesyanoe is a regolith breccia known to contain large concentrations of implanted solar wind gases, whereas noble gas abundances in carbonaceous meteorites show a different, so-called planetary abundance pattern.

The abundances of ^{4}He, ^{20}Ne and ^{36}Ar in Monahans dark regolith are about an order of magnitude lower than those in Pesyanoe, but the relative abundance patterns of the two sample are very similar. For Monahans light, ^{20}Ne is totally cosmogenic and ^{4}He is mainly radiogenic. Any solar ^{20}Ne and ^{4}He would be far less than these measured concentrations. Thus, ^{4}He, and ^{20}Ne in Monahans dark regolith are orders of magnitude more abundant compared to the light phase. ^{36}Ar in Monahans light is ~74% trapped. We conclude that Monahans dark contains moderate concentrations of implanted solar gases. To have acquired this solar gas, some portion of Monahans dark must have resided for a period of time as individual grains on the surface of an H-chondrite parent body regolith. The Monahans clast also indicates a solar gas pattern for He-Ne-Ar, but the concentrations of these gases are a factor of 2–4 lower compared to Monahans dark. This suggests that the dark coloration of the clast is not due to higher concentrations of fine-grained regolith, but may be shock-darkened material produced from the regolith.

Relative abundances of Ar, Kr, and Xe in Monahans samples more closely resemble the pattern seen in carbonaceous chondrites, but the absolute abundances are considerably lower. The absolute abundances of Kr and Xe in Monahans are similar

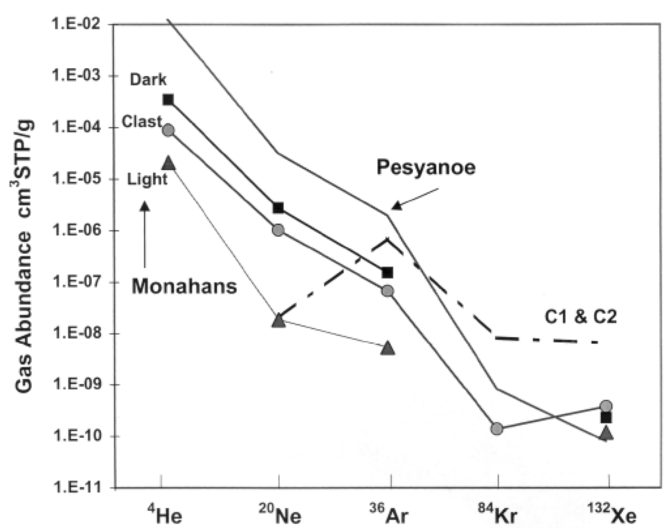

FIG. 2. Relative abundances of the noble gases in three samples of Monahans (light, dark regolith, and a shock-darkened clast) compared to solar wind gases in the Pesyanoe achondrite (Marti, 1969) and "planetary" gases in primitive carbonaceous chondrites (Mazor *et al.*, 1970).

to those of other metamorphosed chondrites that do not contain solar gases. The solar abundance pattern for noble gases is a steep function of mass, whereas this abundance pattern in chondrites is much flatter. (Essentially all trapped noble gases in Pesyanoe are solar-derived.) Thus, the solar gases dominate the Monahans dark inventory at He, Ne, and Ar, but "planetary" gases tend to dominate at Kr and Xe.

The isotopic composition of neon in Monahans samples indicate the presence of two distinct solar gas components, solar wind and solar energetic particles. Figure 3 is a three-isotope plot of Ne for all extractions of the three Monahans samples. The compositions of Ne for the Earth's atmosphere, the solar wind (SW), and the energetic solar component (SEP) are also indicated (Pepin, 1991; Benkert *et al.*, 1993). The first temperature extraction of the dark regolith phase plots near the SW composition. As Ne extraction continues, the $^{20}Ne/^{22}Ne$ ratio moves downward toward the SEP composition, then down a mixing curve toward the cosmogenic composition in the lower right of the figure. This change in Ne composition with temperature has been observed previously in solar-irradiated lunar and meteoritic samples (Murer *et al.*, 1997; Benkert *et al.*, 1993) and occurs because the SW component is located only on grain surfaces, the SEP component is implanted to a depth of microns, and the cosmogenic component is volume-located throughout the silicate grains. The Monahans black clast sample shows similar changes in Ne composition throughout gas extraction to that of the dark regolith. The cosmogenic Ne composition produced during space irradiation of Monahans is defined by the melt extraction of the light phase, which released 96% of the cosmogenic Ne in this sample and gives $^{21}Ne/^{22}Ne = 0.932$. (The 500 °C extraction of the light phase gives a lower $^{21}Ne/^{22}Ne$ value of 0.821, probably due to preferential release of cosmogenic Ne produced from Na and the presence of terrestrial or solar Ne.) Intermediate and higher temperature extractions from all three Monahans samples define a common mixing line (Fig. 3) between the

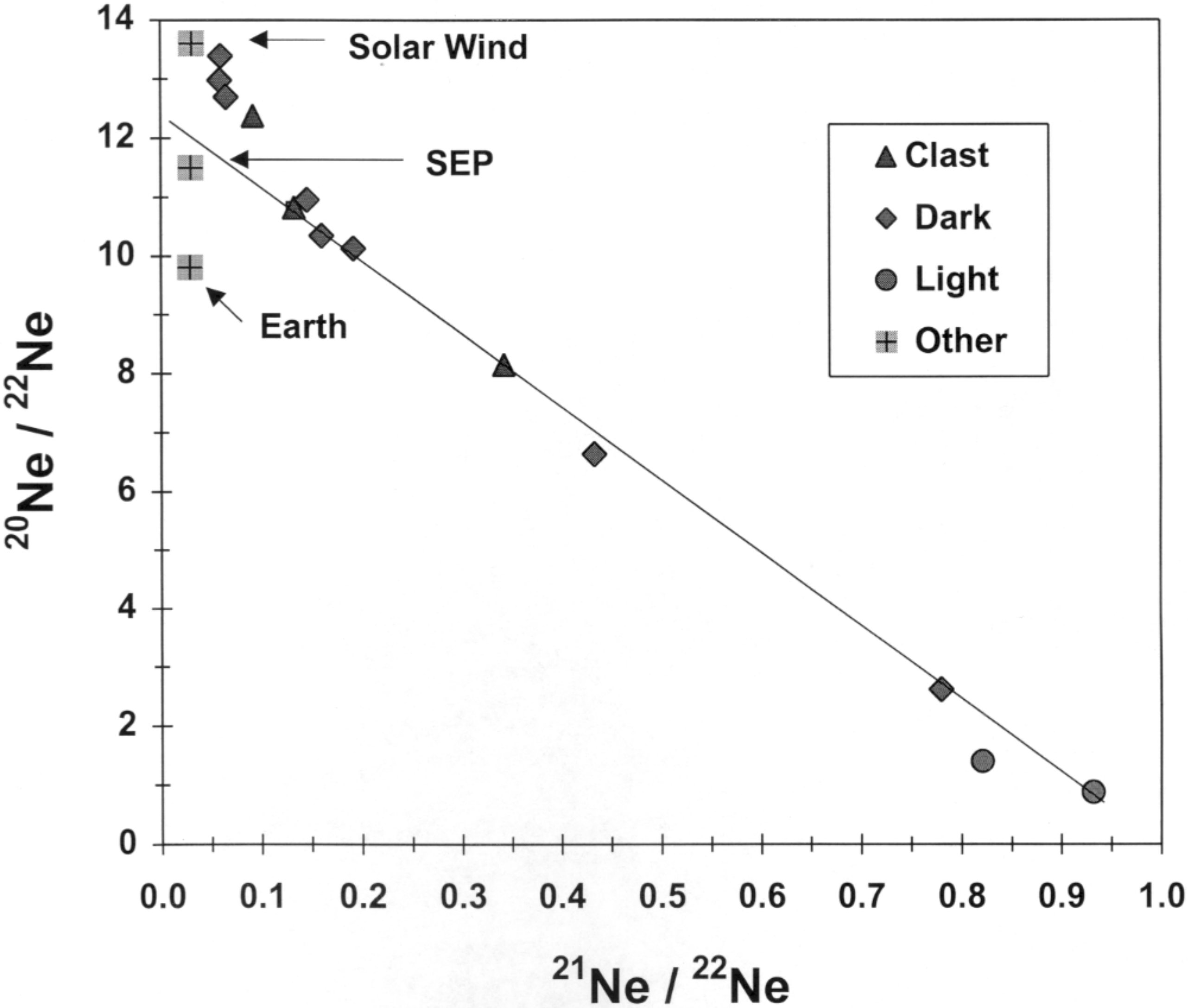

FIG. 3. Neon three-isotope correlation plot for stepwise temperature release of three Monahans samples. Neon compositions of the solar wind, solar energetic particles (SEP) and the Earth's atmosphere are indicated.

cosmogenic composition and a solar composition that appears to be dominated by SEP-Ne over SW-Ne. This suggests that a significant fraction of the originally implanted SW-Ne has been lost by diffusion, as commonly occurs for lunar samples (Benkert *et al.*, 1993).

Cosmogenic Noble Gases and Exposure Ages

Concentrations of cosmic-ray-produced ^{3}He, ^{21}Ne, and ^{38}Ar in the Monahans light phase are given in Table 2. Measured ^{3}He, ^{21}Ne, and ^{22}Ne are entirely cosmogenic in origin, and measured ^{38}Ar was corrected for a small trapped component assuming ^{36}Ar/^{38}Ar = 5.3. To calculate a space, cosmic-ray exposure age from these data, we must adopt a set of cosmogenic production rates. First, we used production rates given by Eugster (1988) for H-chondrites, except that the ^{38}Ar production rate was lowered by 11%, as suggested by Graf and Marti (1995). We used the measured cosmogenic ^{22}Ne/^{21}Ne ratio of 1.072 to normalize for shielding. The calculated ^{3}He, ^{21}Ne, and ^{38}Ar cosmic-ray exposure ages for the light phase are 5.1–6.1 Ma (Table 2).

Next we used H-chondrite production rates of Wieler *et al.* (1996), assuming irradiation in the center of a spherical object which produces ^{22}Ne/^{21}Ne = 1.072. For ^{3}He, ^{21}Ne, and ^{38}Ar, the Wieler *et al.* (1996) model predicts meteoroid radii of ~35–45 cm. An H-chondrite of 40 cm radius would have a mass of ~10^{3} kg, which would be the minimum mass that could produce a ^{22}Ne/^{21}Ne ratio as small as that measured. As the recovered mass of Monahans was only 2.6 kg, considerable ablation loss during atmospheric passage is indicated. The production rates of Wieler *et al.* (1996) give Monahans exposure ages of 5.6–6.4 Ma (Table 2), slightly higher than those calculated above. We prefer the production rates of Wieler *et al.* (1996) because they permit more precise corrections for shielding in moderately large objects, whereas the ^{21}Ne production rate of Eugster (1988) tends to be high (and the age low) as the ^{22}Ne/^{21}Ne ratio decreases below ~1.09. These exposure ages are the minimum possible for the case where ^{22}Ne/^{21}Ne = 1.072. If we assume that Monahans resided within a much larger object of, for example, one meter diameter (equivalent to a 15×10^{3} kg sphere), the Wieler *et al.* (1996) production rates decrease and the ages become ~8–10 Ma. There is no evidence that Monahans derived from such a very large object, although determination of radionuclide concentrations would address the issue. We conclude that the probable space irradiation time for the Monahans meteorite was 6.0 ± 0.5 Ma, but a somewhat longer age is possible if Monahans was a very large object. The Monahans space exposure age lies within a 5–9 Ma peak in exposure ages observed for H-chondrites (Graf and Marti, 1995).

TABLE 2. Exposure ages (Ma) of Monahans.

Isotope	^{3}He	^{21}Ne	^{22}Ne/^{21}Ne	^{38}Ar
Light phase*	91.9	18.7	1.072	2.84
Dark phase*	–	36.8	~1.27	4.3–6.8
Light age (1)	5.8	5.1	–	6.1
Light age (2)	6.3	5.6	–	6.4
Regolith age (3)	–	>13	–	–
Regolith age (4)	–	~18	–	–

*These are cosmogenic gas concentrations of light and dark phases in units of 10^{-9} cm^{3}STP/g. Light-phase space exposure ages (Ma) are calculated assuming production rates from (1) Eugster (1988) and Graf and Marti (1995) and (2) Wieler *et al.* (1996). Regolith exposure ages are (3) minimum value assuming maximum ^{21}Ne production rate for 2π irradiation, and (4) value for 2π irradiation at a depth of a few centimeters.

Calculated concentrations of cosmogenic ^{21}Ne and ^{38}Ar in the Monahans dark regolith phase are also given in Table 2. Cosmogenic ^{21}Ne is ~83% of the total ^{21}Ne, and its concentration varies only slightly whether we assume trapped Ne has the composition of SW or SEP Ne. The solar wind ^{36}Ar/^{38}Ar is not accurately known over the range of ~5.5–5.8 (Pepin *et al.*, 1999). The SEP ^{36}Ar/^{38}Ar is ~4.9 (Rao *et al.*, 1991). However, trapped ^{36}Ar/^{38}Ar in Monahans dark cannot have the pure SEP composition, because several extractions give ratios larger than 4.9. This includes the 750 °C extraction with a ratio of 5.28, which is a minimum value for trapped ^{36}Ar/^{38}Ar in this sample. Consequently, we calculate rather different cosmogenic ^{38}Ar concentrations of 4.3 and 6.8 × 10^{-9} cm^{3}/g assuming trapped ^{36}Ar/^{38}Ar of 5.7 and 5.28, respectively (Table 2). (Assuming trapped ^{36}Ar/^{38}Ar = 5.5 gives $^{38}Ar_{cos} = 5.7 \times 10^{-9}$ cm^{3}/g.) These cosmogenic ^{38}Ar concentrations are only ~13–17% of the total ^{38}Ar.

Solar-implanted ^{4}He/^{3}He ratios in lunar samples and meteorites show a wide range of ~1800 to ~4000, whereas the cosmogenic ratio is ~4. The measured ^{4}He/^{3}He of 16.9 in Monahans dark indicates a substantial trapped He component. Given the uncertainty in trapped ^{4}He/^{3}He and the presence of radiogenic ^{4}He, the concentration of cosmogenic ^{3}He in Monahans dark cannot be reliably calculated.

Concentrations of cosmogenic ^{21}Ne and ^{38}Ar in Monahans dark are twice as large as those in Monahans light (Table 2). The concentration of cosmogenic ^{21}Ne in the black clast (28.4×10^{-9} cm^{3}/g) is intermediate between that of the light and dark regolith phases. With the reasonable assumption that space exposure produced identical concentrations of cosmogenic gases in the light and dark phases, we can subtract the light cosmogenic concentrations from the dark concentrations to determine that excess cosmogenic component produced prior to ejection of Monahans into space. This excess cosmogenic component was produced in the regolith phase during earlier exposure on the H-chondrite parent body surface.

The cosmogenic ^{22}Ne/^{21}Ne ratio for Monahans dark can give information about the shielding conditions of the regolith irradiation, but calculation of this ratio is sensitive to the trapped Ne composition. No single trapped composition gives a consistent $(^{22}Ne/^{21}Ne)_{cos}$ ratio across all temperature extractions. It is obvious that solar wind $^{20}Ne/^{22}Ne$ ratios of >13 are characteristic of the early extractions and an SEP component is also released in later extractions (Fig. 3). The 1050 and 1300 °C extractions released 67% of the total ^{21}Ne. We assumed a two-component trapped and cosmogenic mixture of Ne and iterated the trapped Ne composition until the calculated $(^{22}Ne/^{21}Ne)_{cos}$ ratio was the same for these two extractions. At trapped $^{20}Ne/^{22}Ne$ = 12.1 and $^{21}Ne/^{22}Ne$ = 0.032, $(^{22}Ne/^{21}Ne)_{cos}$ = 1.17 for both extractions. (The calculation is sensitive to our choice of trapped $^{20}Ne/^{22}Ne$, but not to $^{21}Ne/^{22}Ne$.) Because this derived $(^{21}Ne/^{22}Ne)_{cos}$ value contains ^{21}Ne produced in approximately equal amounts in the space and regolith irradiations, and because the space irradiation produced $(^{22}Ne/^{21}Ne)_{cos}$ = 1.07, the $(^{22}Ne/^{21}Ne)_{cos}$ value in the regolith irradiation must be ~1.27. We can use semi-empirical ^{21}Ne production rate models (Reedy, 1985; Graf *et al.*, 1990; Wieler *et al.*, 1996) to estimate the amount of shielding required to produce a ratio of 1.27 during 2π irradiation of a H-chondrite parent body surface. The amount of shielding depth required is very small, <3 cm. Even the measured $(^{22}Ne/^{21}Ne)_{cos}$ of 1.17 would indicate a shielding depth of only ~5 cm. In the next section we will discuss independent evidence from neutron capture products of very low shielding during regolith irradiation of Monahans.

We can use ^{21}Ne production rates from these models to calculate the likely exposure time for the Monahans dark sample while residing in its parent body regolith. The model of Wieler *et al.* (1996) predicts the maximum ^{21}Ne production rate for 2π irradiation of an H-chondrite regolith to be ~1.4×10^{-9} cm^3 STP/g and to occur at a shielding depth of ~50 g/cm^2. (This value is identical to model depth-production calculations we present later.) Combining this rate with the excess ^{21}Ne concentration in Monahans dark gives a minimum regolith exposure age of ~13 Ma. If we assume the irradiation depth to have been only a few cm, we calculate a regolith exposure time of ~18 Ma. For all shielding depths down to ~180 g/cm^2, the regolith exposure time would be in the range ~13–18 Ma. If this regolith exposure occurred early in the parent body history, as we believe, the Monahans breccia must have been stored in the interim at depths of at least several meters to avoid accumulating additional cosmic-ray products.

Thermal Neutron Fluence In Halite

Large concentrations of ^{36}Ar (3.29×10^{-6} cm^3/g) and ^{38}Ar (10.2×10^{-6} cm^3/g) in the Monahans halite sample (Appendix 1) were produced by thermal neutron capture on ^{35}Cl and ^{37}Cl, respectively. These Ar concentrations exceed by orders of magnitude those expected from high energy reactions caused by cosmic rays (compare Table 2). Production of ^{36}Ar is favored over production of ^{38}Ar from a common source of thermal neutrons by about a factor of ~230. However, the two Ar isotopes in Monahans were produced by different neutron sources. Because ^{38}Cl has a half-life of only 37 min before it decays to ^{38}Ar, essentially all of the ^{38}Ar was produced during irradiation in the reactor through neutron capture on ^{37}Cl. Neutron capture by ^{35}Cl produces ^{36}Cl with a half-life of 3.0×10^5 year, which ultimately decays to ^{36}Ar. A negligible amount of that ^{36}Cl produced during reactor irradiation decayed to ^{36}Ar prior to sample analysis. Thus, all of the ^{36}Ar present in the halite was produced from neutrons generated during cosmic-ray irradiation of Monahans, where sufficient time was involved that the ^{36}Cl decayed. Because the ^{35}Cl isotopic abundance is 3× the ^{37}Cl abundance and because the ^{35}Cl cross section for neutron capture is approximately 77× larger than that for ^{37}Cl, the amount of ^{38}Ar produced during cosmic-ray irradiation is negligible compared to that ^{38}Ar produced in the reactor.

From the ^{38}Ar measured in the halite we can calculate the Cl concentration of this sample as a check on Ar retention. We have determined a Cl concentration of 65 ± 5 ppm for the NL-25 hornblende used as a standard in all of our irradiations (Garrison *et al.*, 2000). From ^{38}Ar produced from neutron capture on ^{37}Cl in the halite and hornblende samples in the same irradiation, we calculate a Cl concentration for the halite sample of 33%. This is lower by a factor of 1.8 than the 60.7% Cl concentration of pure NaCl. It is possible that other phases present in our halite sample could have modestly lowered the Cl concentration, but a factor of 1.8 seems very unlikely. (Ca in the halite was ~0.05%.) Self shielding of the halite during irradiation is small and also cannot have produced the observed effect. It is conceivable that part of the halite sample dissolved in the ambient atmospheric humidity and released some Ar between irradiation and sample analysis. On the other hand, analyses of two Monahans halite samples in Zurich (Wieler *et al.*, 2000; R. Wieler, pers. comm.) gave ^{36}Ar concentrations of 3.2 and 2.8×10^{-6} cm^3/g, similar to our measured value of 3.3×10^{-6} cm^3/g. Note that loss of Ar after irradiation does not affect the ^{39}Ar-^{40}Ar age discussed above, although ^{40}Ar loss observed in the halite (Fig. 1c) may have occurred by partial dissolution prior to sample irradiation.

Neutron capture by ^{35}Cl is inversely proportional to neutron energy with minor contribution from epithermal capture resonances. Further, in a large object the maximum neutron flux (n/cm^2/s) occurs near thermal energies (Lingenfelter *et al.*, 1972; Spergel *et al.*, 1986). Thus most ^{36}Cl is produced by thermalized neutrons. The equation describing this neutron capture reaction is $\phi = (^{36}Ar/^{35}Cl) \times \sigma$, where ϕ is thermal neutron fluence in n/cm^2, σ is the neutron capture cross section, and ^{36}Ar and ^{35}Cl are atomic abundances. From this relationship we calculate a thermal neutron fluence observed by Monahans halite of $(2.5–4.5) \times 10^{14}$ n/cm^2 (Table 3). The lower and upper values of this range in fluence correspond to the measured ^{36}Ar concentration and to a value higher by a factor of 1.8, respectively, to allow for the uncertainty in ^{36}Ar concentration of the halite discussed above. We believe this value may be the first reported determination of neutron fluence for a chondrite parent body regolith. (Whitby *et al.* (2000)

TABLE 3. Thermal neutron fluences and fluxes.

Object	Fluence (n/cm^2)	Flux ($n/cm^2/s$)
Monahans halite	2.5–4.5 × 10^{14}	~0.6–1.1*
(H-chondrite regolith)	–	~0.4–0.7†
Few large meteorites‡	0.05–1.3 × 10^{16}	~2.8–5.8
(Space Exposure)		
Lunar soils§	2–6 × 10^{16}	~6–12 at 10^8 years
(Regolith exposure)	–	~0.6–1.2 at 10^9 years

The lower fluence and flux for Monahans were derived from measured ^{36}Ar, whereas the higher values allow for the possibility of some Ar loss from halite.
*Flux at ~50 g/cm^2 shielding depth
†Flux at ~4 g/cm^2 shielding depth.
‡Bogard *et al.* (1995b).
§Russ *et al.* (1972).

report a nearly identical thermal fluence of 2 × 10^{14} n/cm^2 for halite in the Zag H-chondrite, but state that the irradiation could have occurred either during space transit or in the regolith.) Several determinations (by various techniques) of neutron fluence in meteorites during their space exposure as large objects have been reported and give values of (~5–123) × 10^{14} n/cm^2 (Bogard *et al.*, 1995b). Several determinations of neutron fluence for lunar regolith samples commonly fall in the range of (2–6) × 10^{16} n/cm^2 (*e.g.*, Curtis and Wasserburg, 1975). Many of these prior determinations of neutron fluence exceed that measured here for Monahans halite by factors of 10–100. Measurement of a relatively low neutron fluence in the halite is possible because of the very great concentration of Cl in the NaCl phase.

If we assume that the halite was irradiated in Monahans regolith for the same time period as the silicate (see later discussion), we can use the minimum regolith exposure age (Table 2) to calculate the maximum neutron flux. Thus, an irradiation time of ≥13 Ma gives a thermal neutron flux of ≤0.6–1.1 n/cm^2/s, where the range in flux arises from the uncertainty in ^{36}Ar concentration in the halite discussed above. At a shielding depth of only a few centimeters, the flux is ~0.4–0.7 n/cm^2/s. A few large meteorites with measurable neutron-capture effects deriving from space irradiation give thermal neutron fluxes of ~2.8–5.8 n/cm^2/s (Bogard *et al.*, 1995b). Neutron fluxes seen by bulk lunar soils are difficult to determine because loss of noble gases during soil maturation makes the total cosmic-ray exposure times of lunar soils uncertain. Lunar soil exposure ages of 10^8 and 10^9 years imply lunar surface thermal neutron fluxes of ~10 and ~1 n/cm^2/s, respectively (Table 3). The thermal neutron fluences measured in lunar soils are lower than would be predicted from direct measurement of thermal neutron fluence on the lunar surface and imply that lunar soils were irradiated for shorter times than the formation age of the surface rocks from which the soils were produced (Woolum *et al.*, 1973).

IRRADIATION OF THE H-CHONDRITE REGOLITH

The thermal neutron fluence determined for Monahans (and Zag) halite occurred during regolith exposure on the H-chondrite parent body (see below). To use these data to place constraints on the irradiation conditions of the Monahans regolith requires that we consider production rates of cosmogenic ^{21}Ne and neutron-capture ^{36}Cl as a function of shielding depth. In this section we first present model calculations of the depth production of these nuclides. We then show that calculated depth-profiles for 4π space irradiation of large chondrites are consistent with existing data on a large L-chondrite, but are not consistent with production of ^{36}Ar in Monahans halite during space exposure. Finally, we will compare the Monahans data with model calculations of ^{36}Cl and ^{21}Ne depth-production profiles from 2π irradiation of an H-chondrite regolith in order to place constraints on regolith irradiation conditions for Monahans.

^{36}Cl and ^{21}Ne Depth-Production Profiles

Predicting the production rate of a given cosmogenic nuclide as a function of shielding requires cross section data on specific nuclear reactions producing that nuclide, a model for conversion of high-energy cosmic-ray protons into protons and neutrons of intermediate and lower energies through nuclear interactions, and, in the case of neutron-capture products, a neutron transport code to calculate the distribution of neutrons at lower energies. Using this general approach, many previous investigations have calculated depth profiles for a host of nuclides produced by cosmic-ray interactions (Reedy, 1985; Michel *et al.*, 1991, 1996; Reedy *et al.*, 1993; Masarik and Reedy, 1994; Michlovich *et al.*, 1994; Sarafin *et al.*, 1995). We have used the latest versions of these input parameters to calculate the depth production rates of cosmogenic ^{21}Ne and neutron-capture ^{36}Cl for 2π irradiation of a H-chondrite regolith and for 4π space irradiation of an L-chondrite having a radius of 300 g/cm^2 (Fig. 4). Details of the calculations are explained, for example, in Masarik and Reedy (1994). These depth profiles in chondrites are similar to results of some previous calculations (*e.g.*, Spergel *et al.*, 1986; Reedy *et al.*, 1993; Wieler *et al.*, 1996; Michlovich *et al.*, 1994). Because of ~3–4% statistical errors in the calculations, the production curves show some scatter at larger depths in 300 g/cm^2 objects (Fig. 4, top). We made calculations for both H- and L-chondrites under each (2π and 4π) shielding condition, and found the results between H- and L-chondrites to differ by less than the statistical variations.

The depth production rates of ^{36}Cl from thermalized neutrons reach similar maximum values for 2π regolith irradiation and 4π irradiation of a 300 g/cm^2 chondrite, but these occur at different shielding depths of ~150 and ~275 g/cm^2, respectively (Fig. 4). Depth production of cosmogenic ^{21}Ne differs much more between the two irradiation conditions. For

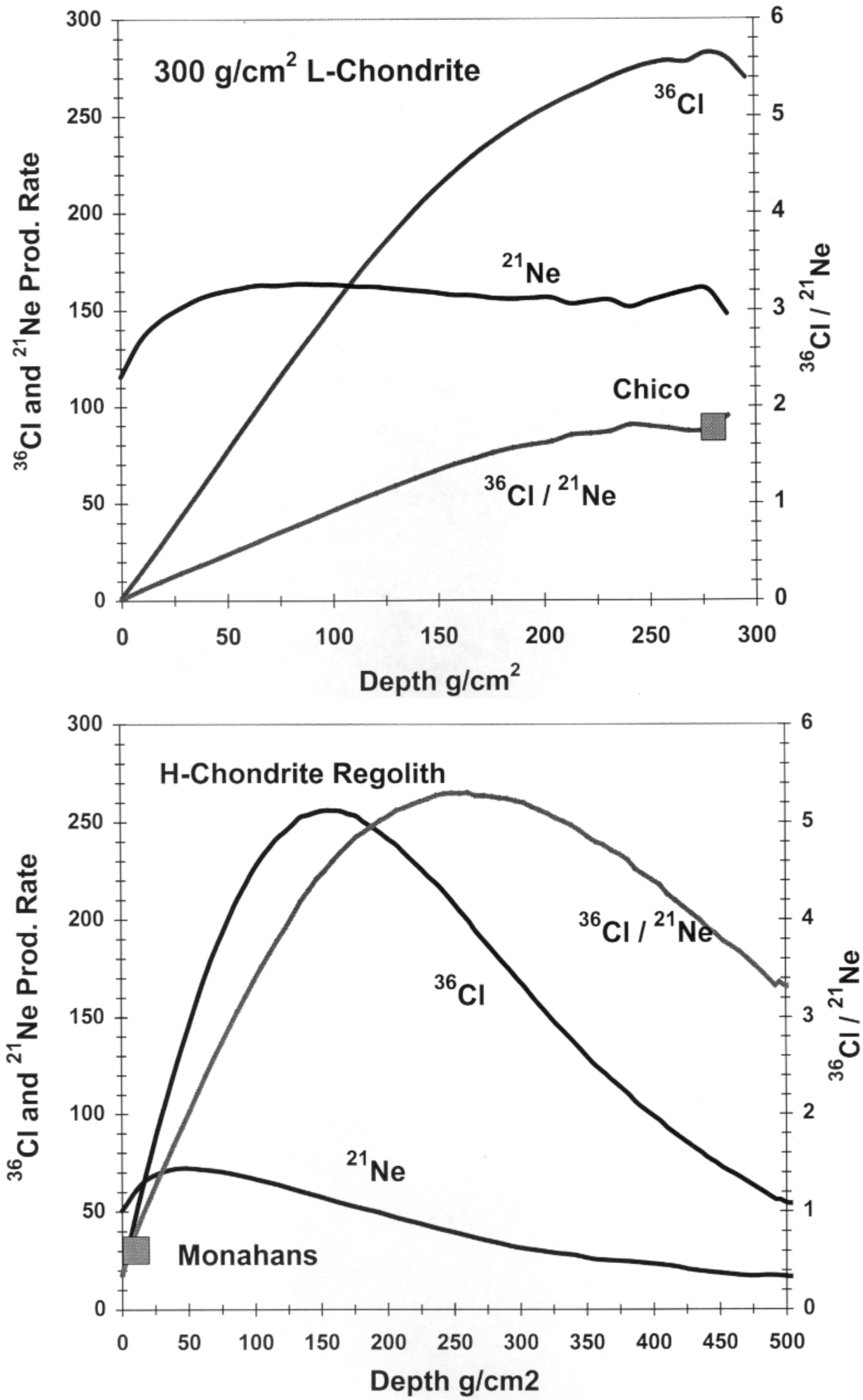

FIG. 4. Plot of the calculated production rates (left scale) of neutron-capture ^{36}Cl (atoms/min/g-Cl) and cosmogenic ^{21}Ne (atoms/min/kg-sample) and of the $^{36}Cl_n/^{21}Ne_{cos}$ ratio (right scale) for (top) an L-chondrite of 300 g/cm^2 radius and (bottom) 2π surface irradiation of an H-chondrite parent body. The measured $^{36}Ar_n/^{21}Ne_{cos}$ ratios (where $^{36}Ar_n$ represents the integrated ^{36}Cl production) for the Chico L-chondrite and Monahans dark regolith are shown on the appropriate figure.

300 g/cm^2 chondrites, $^{21}Ne_{cos}$ quickly rises to a broad maximum at 75–100 g/cm^2, then slowly decreases with depth. For 2π irradiation, $^{21}Ne_{cos}$ production reaches its maximum at ~50 g/cm^2, then decreases more quickly with depth. The maximum $^{21}Ne_{cos}$ for 2π irradiation is only ~44% as large as the maximum $^{21}Ne_{cos}$ in 4π irradiation. As a consequence of these differences, the $^{36}Cl/^{21}Ne$ ratios have quite different depth profiles for the two cases (Fig. 4). For 300 g/cm^2 chondrites, the $^{36}Cl/^{21}Ne$ ratio begins at ~0.1 at the surface and increases steadily with depth to a maximum value of 1.8 at the meteorite center (Fig. 4, top). For 2π irradiation, the $^{36}Cl/^{21}Ne$ ratio begins at ~0.4 at the surface and increases steadily to a maximum value of 5.3 at a shielding depth of 250 g/cm^2. The ratio then decreases more slowly to a value of 3.4 at a shielding depth of 500 g/cm^2. These results mean that the $^{36}Cl/^{21}Ne$ ratio in an irradiated object can be a sensitive indicator of shielding depth.

We first examine $^{36}Cl/^{21}Ne$ ratios for the case of space irradiation of the large Chico L-chondrite. Bogard *et al.* (1995b) reported thermal neutron fluences and fluxes arising from space irradiation of several large chondrites, including Chico (Table 3). Two Chico measurements gave an excess ^{36}Ar concentration of ~3×10^{-8} cm^3/g, which was produced from neutron capture on ^{35}Cl. The same two Chico samples gave an average Cl concentration of 96 ppm (Garrison *et al.*, 2000). Combining these Chico data gives 3.1×10^{-4} cm^3 of $^{36}Ar_n$ per gram of Cl. Because the measured $^{36}Ar_n$ gives the time-integrated ^{36}Cl production, we can use a space exposure age for Chico of ~65 Ma (Garrison *et al.*, 1992) to calculate a ^{36}Cl production rate of ~245 atoms/min/g-Cl (cf., Fig. 4, top). Garrison *et al.* (1992) reported cosmogenic noble gases for several samples of Chico, including an average cosmogenic ^{21}Ne concentration of 18.5×10^{-8} cm^3/g for the two samples for which $^{36}Ar_n$ was determined. Combining these data gives a $^{36}Ar_n/^{21}Ne_{cos}$ ratio for Chico of 1.8. Because the units for this ratio are the same as those used in Fig. 4, we can plot this ratio for Chico on the $^{36}Cl/^{21}Ne$ production curve for large L-chondrites (Fig. 4, top). Chico plots at the highest predicted ratio and greatest shielding depth on the model curve and is consistent with previous conclusions from radionuclide and $^{22}Ne/^{21}Ne$ data that Chico was irradiated in space as a large object (Garrison *et al.*, 1992).

We now use $^{36}Ar_n/^{21}Ne_{cos}$ to examine possible irradiation conditions for Monahans. We consider only that $^{21}Ne_{cos}$ produced during irradiation in the parent body regolith (1.81×10^{-8} cm^3/g; Table 2) and assume that $^{36}Ar_n$ in Monahans halite was produced in the same regolith irradiation. We adopt $^{36}Ar_n = 3.29 \times 10^{-6}$ cm^3/g (the measured halite value), to obtain 5.4×10^{-6} cm^3 of $^{36}Ar_n$ per g-Cl. These values yield a $^{36}Ar_n/^{21}Ne_{cos}$ production ratio for Monahans regolith of 0.3, where the units are the same as those used in Fig. 4. (If we used a $^{36}Ar_n$ abundance larger by a factor of 1.8 to compensate for possible Ar loss (see above discussion), the $^{36}Cl/^{21}Ne$ ratio becomes 0.5.) The Monahans value of this ratio plots on the $^{36}Cl/^{21}Ne$ curve for 2π regolith irradiation (Fig. 4, bottom) at a depth of only ~3 g/cm^2 and is similar to the smallest $^{36}Cl/^{21}Ne$ predicted by the model calculations.

The position of the Monahans $^{36}Cl/^{21}Ne$ value on the model curve in Fig. 4 (bottom) rules out any possibility that $^{36}Ar_n$ in the halite was produced during the 4π space exposure. Because the excess $^{21}Ne_{cos}$ in Monahans dark phase must have been produced during regolith irradiation, and because the Monahans $^{36}Ar_n/^{21}Ne_{cos}$ ratio implies that the minimum amount of ^{36}Cl that could be produced during this regolith irradiation is just the amount observed, little of the ^{36}Cl could have been produced during space exposure. Stated in another way, if a significant fraction of the ^{36}Cl in Monahans halite were produced during space exposure, the amount produced during regolith exposure would be too little to be consistent with the model depth production curves for any depth. The conclusion that $^{36}Ar_n$ was produced during regolith irradiation is not surprising. Unlike Chico, the cosmogenic $^{22}Ne/^{21}Ne$ ratio for Monahans light does not suggest a sufficiently large body to produce a high thermal neutron flux, and the space exposure age of Monahans does not seem sufficiently long to produce a high neutron fluence.

Monahans Regolith Irradiation Models

The I-Xe dating results of Whitby *et al.* (2000) show that formation of halite present in the Zag H-chondrite occurred very early. Because halite grains are fragile and are expected to be destroyed relatively quickly at parent body surfaces, the preservation of halite in Monahans and Zag is further evidence that this regolith irradiation occurred early in parent body history. The 4.53 Ga Ar-Ar age of Monahans light may approximate the time this surface regolith existed.

To utilize the $^{36}Ar_n$ and $^{21}Ne_{cos}$ data for Monahans to constrain irradiation conditions on the parent body regolith requires consideration of possible irradiation models for silicate and halite. There are three basic classes of models, which cover whether the silicate and halite were irradiated at common shielding depths or not and whether they were irradiated for common times or not. These irradiation models may also help differentiate between the two possible origins suggested for Monahans halite: dissolution and precipitation by water flowing within the parent asteroid, or delivery to the regolith surface from an outside source such as a salt-containing icy object (Zolensky *et al.*, 1999a).

The first irradiation option, that halite and silicate were irradiated at a common depth for a common time, places specific and interesting constraints on the Monahans regolith irradiation history and is the irradiation option addressed directly by Fig. 4, bottom. Identical time and depth of irradiation for halite and silicate imply that both phases were introduced into the regolith from subsurface rock, and thus that the halite was formed in the outer portions of the H-chondrite parent by the action of liquid water (Zolensky *et* *al.* (1999a). Because of the relatively low measured $^{36}Cl/^{21}Ne$ ratio in Monahans halite and silicate compared to the production *vs.* depth model curve, all regolith irradiation is required to have occurred within the uppermost few cm for a time period of ~18 Ma. This constraint implies that this H-chondrite parent body regolith was thin, probably no more than a few tens of cm deep. Regoliths are developed from impacts into underlying bedrock, and a deep mature regolith is expected to exhibit characteristics of long irradiation times and extensive mixing, as is the case for regoliths developed on lunar mare. Some early theoretical models of asteroid regoliths predicted thin regoliths (Chapman, 1976), but recent flybys of a few asteroids suggest the likely presence of substantial regoliths (Greenberg *et al.*, 1994). We envision that a regolith developed on a fresh rock surface for ~18 Ma on the early H-chondrite parent asteroid, then was deeply covered by ejecta from a very large impact and protected from cosmic rays and major impacts until Monahans was ejected into space as a meteorite ~6 Ma ago. It is likely that the Monahans regolith represents a transient surface on the parent body, and different transient surfaces may have been sampled by other regolith-containing H-chondrites. This process of development of a thin regolith and subsequent burial may have occurred over and over in early solar system history when large impacts were more common. In more recent times, however, large impacts have been less common, and surface regoliths on asteroids have more time for development as a result of smaller impacts. Such a time evolution of regolith production apparently occurred on the Moon. Mare surfaces in existence for the past ~3.8 Ga have regoliths that are a few meters deep but very mature regoliths. Older highland surfaces, however, have deeper and much less mature mega-regoliths, produced by the higher rate of large impacts >3.8 Ga ago (McKay *et al.*, 1986).

The second regolith irradiation option, that halite had a different irradiation time at the same depth compared to the silicate, also suggests a thin regolith. A longer irradiation time for the halite than for the silicate at a common shielding depth cannot produce $^{36}Cl/^{21}Ne$ ~0.3, and thus can be ruled out. However, a shorter irradiation time for the halite than for the silicate at a common shielding depth could, in principle, produce the observed $^{36}Cl/^{21}Ne$ in Monahans. For example, irradiation at a common shielding depth of ~180 g/cm^2 for a time period of ~18 Ma for the silicate but only ~1 Ma for the halite would produce $^{36}Cl/^{21}Ne \cong 0.5$. However, most of these combinations of irradiation time would violate the conclusion made from $(^{21}Ne/^{22}Ne)_{cos}$ in the dark phase that silicate irradiation occurred at shallow depth. With the constraint from Ne that the silicate was irradiated in a shallow regolith, halite irradiation in this regolith also would have to occur under low shielding, even if for a shorter time period. This suggests that, under a simple irradiation model, the halite was probably not added from an outside source after formation of the regolith.

The third option, halite and silicate irradiation at different depths for a common time, is possible in principle, but seems relatively unlikely for the reason that it would tend to produce a $^{36}Cl/^{21}Ne$ in Monahans greater than that observed. For example, given the measured $^{36}Cl/^{21}Ne$ in Monahans of 0.3–0.5, silicate irradiation at a depth corresponding to the maximum in the ^{21}Ne production rate would also permit the largest ^{36}Cl production rate and greatest halite irradiation depth. If we combine the ^{21}Ne production rate of ~72 atoms/min/kg at ~50 g/cm^2 with a $^{36}Cl/^{21}Ne$ ratio of 0.5, the ^{36}Cl production rate would have to be ~36 atoms/min/g-Cl. From the model curve (Fig. 4, bottom) this rate is predicted to occur only for regolith depths of <7 g/cm^2. Silicate irradiation at other depths make the situation worse. For example, the ^{21}Ne production rate at 300 g/cm^2 (~31 atoms/min/kg) would require the ^{36}Cl production rate in Monahans halite to be only ~16 at/min/g-Cl (cf., Fig. 4, bottom). Both of these assumed greater silicate irradiation depths are inconsistent with evidence from $(^{21}Ne/^{22}Ne)_{cos}$ presented earlier that the silicate was irradiated at shallow depths. If we restrict ^{21}Ne production to near-surface regions, production of ^{36}Cl is also restricted to near-surface regions, which is the situation considered under the first irradiation option above.

In summary, the relatively simple regolith irradiation models examined above suggest that the silicate and halite comprising the Monahans dark phase were derived concurrently by impact from the surface rocks of the H-chondrite parent body very early in its history. At that time the halite possibly occurred as small vein deposits in the rocks. A relatively thin surface regolith developed over a period of ~18 Ma, during which time it was irradiated with cosmic-ray protons. Most likely the silicate and halite were irradiated for a common time at similar shallow depths. Subsequently, this regolith horizon was deeply buried by a large impact, which also may have mixed previously unirradiated rock clasts with the irradiated material, creating the Monahans breccia. The breccia remained deeply buried until a large impact ~6 Ma ago ejected it into space.

More complex Monahans regolith irradiation model permit different irradiation times and depths for halite and silicate and cannot be excluded based on the Monahans data. Even more complex models, however, do not permit late addition of unirradiated halite to the surface of the silicate regolith, as this would generate a $^{36}Cl/^{21}Ne$ ratio in Monahans lower than that measured. On the other hand, the halite grains could have been irradiated elsewhere in the regolith at some depth having a relatively high ^{36}Cl production rate for a much shorter period time than the silicate was irradiated, and then mixed with the silicate grains by impact. For example, mixing silicate irradiated for 13 Ma at a depth of a few g/cm^2 with halite irradiated for ~3 Ma at a shielding depth of 40 g/cm^2 could give a $^{36}Cl/^{21}Ne$ ratio of 0.5. As the halite irradiation depth increases, however, its irradiation time would have to decrease proportionally. These different irradiation time and depth scenarios imply a complex, possibly deep regolith with a history of differential irradiation and mixing of soil components, as commonly occurs for mature lunar soils (*e.g.*, Heiken *et al.*, 1976). For these more complex regolith models, it is difficult to place constraints on the specific irradiation history of either the silicate or the halite. However, Monahans and most regoliths sampled by meteorites are very immature by lunar soil standards. Thus, to the degree that simpler, less mature regoliths are indicated for Monahans, the data suggest this regolith was probably relatively shallow and that the halite probably was derived from near-surface rocks.

Acknowledgements–We thank Everett Gibson (J. S. C.) and Carleton Moore (A. S. U. Center for Meteorite Studies) for the samples of Monahans silicate and Mike Zolensky (J. S. C.) for the halite sample. R. Burgess, R. Reedy, and R. Wieler are thanked for constructive reviews. Noble gas studies at J.S.C. were supported by NASA RTOP 344-31.

Editorial handling: R. Wieler

REFERENCES

Benkert J. P., Baur H., Signer P. and Wieler R. (1993) He, Ne, and Ar from the solar wind and solar energetic particles in lunar ilmenites and pyroxenes. *J. Geophys. Res.* **98**, 13 147–13 162.

Bogard D. D., Garrison D. H., Norman M., Scott E. R. D. and Keil K. (1995a) ^{39}Ar-^{40}Ar age and petrology of Chico: Large-scale impact melting on the L-chondrite parent body. *Geochim. Cosmochim. Acta* **59**, 1383–1399.

Bogard D. D., Nyquist L. E., Bansal B. M., Garrison D. H., Wiesmann H., Herzog G. F., Albrecht A. A. and Klein J. (1995b) Neutron-capture ^{36}Cl, ^{41}Ca, ^{36}Ar, and ^{150}Sm in large chondrites: Evidence for high fluences of thermalized neutrons. *J. Geophys. Res.* **100**, 9401–9416.

Bogard D. D., Garrison D. H. and McCoy T. J. (2000) Chronology and petrology of silicates from IIE iron meteorites: Evidence of a complex parent body evolution. *Geochim. Cosmochim. Acta* **64**, 2133–2154.

Chapman C. R. (1976) Asteroids as meteorite parent bodies: The astronomical perspective. *Geochim. Cosmochim. Acta* **40**, 701–719.

Curtis D. G. and Wasserburg G. J. (1975) Apollo 17 neutron stratigraphy, sedimentation, and mixing in the lunar regolith. *Moon* **13**, 185–228.

Eugster O. (1988) Cosmic-ray production rates for ^{3}He, ^{21}Ne, ^{38}Ar, ^{83}Kr, and ^{126}Xe in chondrites based on ^{81}Kr-Kr exposure ages. *Geochim. Cosmochim. Acta* **52**, 1649–1662.

Garrison D. H., Bogard D. D., Albrecht A. A., Vogt S., Herzog G. F., Klein J., Fink D., Dezfouly-Arjomandy B. and Middleton R. (1992) Cosmogenic nuclides in core samples of the Chico L6 chondrite: Evidence for irradiation under high shielding. *Meteoritics* **27**, 371–381.

Garrison D., Hamlin S. and Bogard D. (2000) Chlorine abundances in meteorites. *Meteorit. Planet. Sci.* **35**, 419–429.

Graf T. and Marti K. (1995) Collisional history of H chondrites. *J. Geophys. Res.* **100**, 21 247–21 263.

Graf T., Baur H. and Signer P. (1990) A model for the production of cosmogenic nuclides in chondrites. *Geochim. Cosmochim. Acta* **54**, 2521–2534.

Greenberg R., Nolan M. C., Bottke W. F. and Kolvoord R. A. (1994) Collisional history of Gaspera. *Icarus* **107**, 84–97.

Heiken G. H., Morris R. V., McKay D. S. and Fruland R. M. (1976) Petrographic and ferromagnetic resonance studies of the Apollo 15 deep drill core. *Proc. Lunar Sci. Conf.* **7th**, 93–111.

Lingenfelter R. E., Canfield E. H. and Hampel V. E. (1972) The lunar neutron flux revisited. *Earth Planet. Sci. Lett.* **16**, 355–369.

Marti K. (1969) Solar-type xenon: A new isotopic composition of xenon in the Pesyanoe meteorite. *Science* **166**, 1263–1265.

Masarik J. and Reedy R. C. (1994) Effects of bulk composition on nuclide production processes in meteorites. *Geochim. Cosmochim. Acta* **58**, 5307–5217.

Mazor E., Heymann D. and Anders E. (1970) Noble gases in carbonaceous chondrites. *Geochim. Cosmochim. Acta* **34**, 781–824.

McKay D. S., Bogard D. D., Morris R. V., Korotev R. L., Johnson P. and Wentworth S. J. (1986) Apollo 16 regolith breccias: Characterization and evidence for early formation in the mega-regolith. *J. Geophys. Res.* **91**, *Proc. Lunar Planet. Sci. Conf.* **16th**, Suppl. B4, D277–D303.

Michel R., Dragovitsch P., Cloth P., Dagge G. and Filges D. (1991) On the production of cosmogenic nuclides in meteoroids by galactic protons. *Meteoritics* **26**, 221–242.

Michel R., Leya I. and Borges L. (1996) Production of cosmogenic nuclides in meteoroids: Accelerator experiments and model calculations to decipher the cosmic ray record in extraterrestrial matter. *Nucl. Instrum. Methods Phys. Res.* **113**, 434–444.

Michlovich E. S., Vogt S., Masarik J., Reedy R. C., Elmore S. and Lipschutz M. E. (1994) ^{26}Al, ^{10}Be, and ^{36}Cl Depth Profiles in Canyon Diablo Meteorites. *J. Geophys. Res.* **E98**, 23 187–23 194.

Murer C. A., Baur H., Signer P. and Wieler R. (1997) Helium, neon, and argon abundances in the solar wind: In vacuo etching of meteoritic iron-nickel. *Geochim. Cosmochim. Acta* **61**, 1303–1314.

Pepin R. O. (1991) On the origin and early evolution of terrestrial planet atmospheres and meteoritic volatiles. *Icarus* **92**, 2–79.

Pepin R. O., Becker R. H. and Schlutter D. J. (1999) Irradiation records in regolith materials. I: Isotopic compositions of solar-wind neon and argon in single lunar mineral grains. *Geochim. Cosmochim. Acta* **63**, 2145–2162.

Rao M. N., Garrison D. H., Bogard D. D., Badhwar G. and Murali A. V. (1991) Composition of solar flare noble gases preserved in meteorite parent body regolith. *J. Geophys. Res.* **96**, 19 321–19 330.

Reedy R. C. (1985) A model for GCR particle fluxes in stony meteorites and production rates of cosmogenic nuclides. *J. Geophys. Res.* **90**, *Proc. Lunar Planet. Sci. Conf.* **15th** Suppl., C722–C728.

Reedy R. C., Masarik J., Nishiizumi K., Arnold J. R., Finkel R. C., Caffee M. W., Southon J., Jull A. J. T. and Donahue D.J. (1993) Cosmogenic radionuclide profiles in Knyahinya: New measurements and models (abstract). *Lunar Planet. Sci.* **24**, 1195–1196.

Russ G. P., III, Burnett D. S. and Wasserburg G. J. (1972) Lunar neutron stratigraphy. *Earth Planet. Sci. Lett.* **15**, 172–186.

Sarafin R., Englert P., Masarik J. and Reedy R. C. (1995) Cosmogenic ^{53}Mn in the Main Fragment of the Norton County Aubrite. *Geochim. Cosmochim. Acta* **59**, 825–830.

Spergel M. S., Reedy R. C., Lazareth O. W., Levy P. W. and Slatest L. A. (1986) Cosmogenic neutron-capture-produced nuclides in stony meteorites. *J. Geophys. Res.* **91**, *Proc. Lunar Planet. Sci. Conf.* **16th** Suppl., D483–D494.

Turner G., Enright M. C. and Cadogan P. H. (1978) The early history of the chondrite parent bodies inferred from ^{40}Ar-^{39}Ar ages. *Proc. Lunar Planet. Sci. Conf.* **9th**, 989–1025.

Whitby J. A., Burgess R., Turner G., Gilmour J. D. and Bridges J. C. (2000) Extinct ^{129}I in halite from a primitive meteorite: Evidence for evaporite formation in the early solar system. *Science* **288**, 1819–1821.

WIELER R. *ET AL.* (1996) Exposure history of the Torino meteorite. *Meteorit. Planet. Sci.* **31**, 265–272.

WIELER R., GÜNTHER D., HATTENDORF B., LEYA I., PETTKE T., VOGEL N. AND ZOLENSKY M. E. (2000) The chemical composition and light noble gas data of halite in the Monahans regolithic breccia (abstract). *Lunar Planet. Sci.* **31**, #1560, Lunar and Planetary Institute, Houston, Texas, USA (CD-ROM).

WOOLUM D. S., BURNETT D. S. AND BAUMAN C. A. (1973) *Lunar Neutron Probe Experiment*. Apollo 17 Preliminary Science Report, NASA SP-330, 18.1–18.12.

ZOLENSKY M. E., BODNAR R. J., GIBSON E. J., NYQUIST L. E., REESE Y., SHIH C. Y. AND WIESMANN H. (1999a) Asteroidal water within fluid inclusion-bearing halite in an H5 chondrite, Monahans (1998). *Science* **285**, 1377–1379.

ZOLENSKY M. E., BODNAR R. J. AND RUBIN A. E. (1999b) Asteroidal water within fluid inclusion-bearing halite in ordinary chondrites (abstract). *Meteorit. Planet. Sci.* **34 (Suppl.)**, A124.

ZOLENSKY M. E., BODNAR R. J., BOGARD D. D., GARRISON D. H., GIBSON E. J., NYQUIST L. E., REESE Y., SHIH C. Y. AND WIESMANN H. (1999c) Fluid inclusion-bearing halite and solar gases in the Monahans 1998 H5 chondrite (abstract). *Lunar Planet. Sci.* **30**, #1280, Lunar and Planetary Institute, Houston, Texas, USA (CD-ROM).

APPENDIX

APPENDIX 1. Ar isotopic data, ^{39}Ar concentrations, K/Ca ratios, and ^{39}Ar-^{40}Ar ages (in Ga) for stepwise temperature extractions of irradiated Monahans samples.

Temperature (°C)	^{39}Ar (10^{-9} cm^3 STP/g)	Age (Ga)	K/Ca ratio (×10)	40/39 ± (×1)	38/39 ± (×100)	37/39 ± (×1)	36/39 ± (×100)
Monahans Light	Wt = 0.04869 g,	*J* = 0.03073 ± 0.00006					
400	5.98	4.619	3.652	388.5	6.86	1.51	16.22
		0.010	0.384	2.2	0.08	0.16	0.28
450	4.73	4.503	3.951	362.4	2.30	1.39	4.54
		0.006	0.041	1.1	0.15	0.01	0.15
500	7.62	4.322	3.970	324.6	1.88	1.39	2.99
		0.005	0.041	0.8	0.14	0.01	0.09
530	7.44	4.346	4.074	329.4	1.72	1.35	2.08
		0.005	0.042	0.7	0.13	0.01	0.09
550	6.18	4.384	4.074	337.1	1.43	1.35	2.23
		0.006	0.042	0.9	0.14	0.01	0.12
575	10.87	4.427	4.027	346.0	1.50	1.37	3.67
		0.004	0.041	0.5	0.13	0.01	0.08
600	12.91	4.473	4.050	355.8	1.68	1.36	5.27
		0.004	0.041	0.4	0.13	0.01	0.07
620	11.46	4.498	3.980	361.3	2.04	1.38	7.62
		0.004	0.040	0.5	0.13	0.01	0.08
635	12.85	4.522	4.191	366.5	1.91	1.31	7.25
		0.004	0.042	0.5	0.13	0.01	0.08
650	14.07	4.524	4.166	366.9	2.02	1.32	7.95
		0.004	0.042	0.5	0.13	0.01	0.08
660	6.21	4.534	4.193	369.1	1.35	1.31	4.08
		0.005	0.043	0.9	0.14	0.01	0.12
675	9.41	4.534	4.111	369.2	1.30	1.34	4.01
		0.004	0.042	0.6	0.13	0.01	0.09
705	14.95	4.531	3.764	368.5	1.52	1.46	4.11
		0.004	0.038	0.4	0.13	0.01	0.06
725	7.63	4.534	3.586	369.2	1.25	1.53	2.10
		0.005	0.037	0.7	0.14	0.02	0.10
740	5.04	4.542	3.225	371.0	1.61	1.71	2.51
		0.006	0.034	1.0	0.15	0.02	0.15
765	5.76	4.529	2.651	368.1	1.87	2.08	3.32
		0.005	0.027	1.0	0.14	0.02	0.13
790	4.44	4.521	1.988	366.3	2.45	2.77	3.65
		0.006	0.021	1.2	0.15	0.03	0.17
850	5.64	4.488	1.169	359.2	4.34	4.71	7.60
		0.006	0.012	1.0	0.15	0.05	0.15

APPENDIX 1. *Continued.*

Temperature (°C)	^{39}Ar (10^{-9} cm^3 STP/g)	Age (Ga)	K/Ca ratio (×10)	40/39 ± (×1)	38/39 ± (×100)	37/39 ± (×1)	36/39 ± (×100)
Monahans Light *(continued)*							
900	3.64	4.315	0.704	323.3	8.75	7.81	17.24
		0.006	0.007	1.0	0.16	0.08	0.14
940	3.70	4.058	0.406	276.1	14.58	13.53	32.36
		0.006	0.004	0.8	0.17	0.14	0.18
975	2.37	3.825	0.297	238.7	13.64	18.52	35.65
		0.007	0.003	0.9	0.19	0.20	0.34
1020	2.08	3.740	0.215	226.2	15.29	25.54	40.96
		0.008	0.002	1.0	0.21	0.28	0.36
1075	4.40	4.069	0.097	278.0	18.11	56.88	39.97
		0.006	0.001	0.8	0.20	0.59	0.30
1125	0.97	4.090	0.033	281.5	45.85	167.94	98.48
		0.018	0.000	3.1	0.72	2.49	1.44
1200	0.75	4.017	0.033	269.1	64.44	166.90	183.35
		0.024	0.001	4.0	1.17	3.01	3.11
1300	1.43	4.343	0.068	328.9	52.07	80.65	171.08
		0.013	0.001	2.5	0.51	1.01	1.52
1400	0.18	4.206	0.081	302.5	84.27	68.09	236.28
		0.066	0.003	12.2	4.34	2.87	11.98
1575	0.04	2.503	0.192	97.8	79.21	28.64	297.72
		0.297	0.043	21.4	24.58	6.45	91.93
Monahans Dark	Wt = 0.05834 g,	*J* = 0.03066 ± 0.00006					
400	16.84	4.714	4.068	412.2	20.63	1.35	39.35
		0.004	0.041	0.5	0.14	0.01	0.08
450	3.06	4.582	4.183	380.8	18.85	1.31	31.28
		0.007	0.045	1.4	0.20	0.01	0.28
505	18.57	4.417	4.025	344.6	29.01	1.37	30.70
	0.00	0.004	0.040	0.3	0.14	0.01	0.07
535	13.25	4.418	3.540	344.9	28.50	1.55	36.17
	0.00	0.004	0.036	0.4	0.14	0.02	0.09
560	12.10	4.430	3.630	347.4	22.05	1.52	45.61
	0.00	0.004	0.037	0.5	0.14	0.02	0.12
600	26.95	4.425	3.496	346.4	29.27	1.57	109.32
	0.00	0.003	0.035	0.3	0.13	0.02	0.15
620	15.09	4.456	4.012	352.9	29.99	1.37	124.50
	0.00	0.004	0.041	0.5	0.15	0.01	0.21
638	14.53	4.469	4.054	355.7	31.33	1.36	126.99
	0.00	0.004	0.041	0.3	0.14	0.01	0.18
655	10.90	4.483	3.991	358.7	25.43	1.38	90.87
	0.00	0.004	0.040	0.6	0.15	0.01	0.22
680	14.13	4.481	3.586	358.4	26.35	1.53	98.79
	0.00	0.004	0.036	0.5	0.15	0.02	0.17
700	6.85	4.503	3.526	363.1	18.82	1.56	63.14
	0.00	0.005	0.036	0.7	0.15	0.02	0.21
725	6.43	4.495	3.027	361.3	21.75	1.82	78.93
	0.00	0.005	0.031	0.8	0.16	0.02	0.24
750	5.69	4.450	2.502	351.6	19.84	2.20	79.96
		0.005	0.026	0.8	0.17	0.02	0.26
790	5.52	4.434	1.738	348.3	17.49	3.16	75.68
		0.005	0.018	0.8	0.16	0.03	0.27
855	7.79	4.304	1.055	321.8	23.44	5.21	99.26
		0.005	0.011	0.7	0.16	0.05	0.30
900	5.90	4.089	0.834	281.9	30.70	6.59	126.92
		0.007	0.009	1.1	0.20	0.07	0.56

APPENDIX 1. *Continued*.

Temperature (°C)	^{39}Ar (10^{-9} cm^3 STP/g)	Age (Ga)	K/Ca ratio (×10)	40/39 ± (×1)	38/39 ± (×100)	37/39 ± (×1)	36/39 ± (×100)
Monahans Dark *(continued)*							
930	4.71	3.939	0.622	256.8	42.12	8.84	177.72
		0.006	0.007	0.8	0.23	0.09	0.65
970	5.76	3.954	0.607	259.2	36.45	9.06	159.31
		0.005	0.006	0.7	0.21	0.09	0.50
1020	7.33	3.899	0.513	250.5	35.97	10.71	154.79
		0.005	0.005	0.5	0.17	0.11	0.42
1100	8.25	3.942	0.155	257.4	51.86	35.48	195.63
		0.005	0.002	0.6	0.24	0.36	0.51
1200	4.46	3.916	0.081	253.3	101.85	67.61	431.64
		0.006	0.001	0.9	0.44	0.72	1.64
1350	1.91	4.043	0.112	274.1	120.28	49.13	503.6
		0.009	0.001	1.4	0.75	0.55	2.9
1575	0.004	8.058	0.071	2806	529	77.9	2077
		0.523	0.021	823	165	22.9	645
Monahans Halite	Wt = 0.00187 g,	*J* = 0.03086 ± 0.00010					
100	0.03	5.745	1.116	750.4	89.4	4.928	210.5
		0.887	0.574	384.9	66.3	2.533	154.2
250	0.95	2.250	12.027	80.4	81.7	0.457	80.6
		0.486	4.551	30.3	43.5	0.173	44.6
500	107.17	1.102	51.356	27.3	292.5	0.107	61.4
		0.032	2.088	1.1	16.2	0.004	3.4
600	394.20	4.124	92.378	286.2	1913.1	0.060	612.1
		0.006	1.001	0.5	4.1	0.001	1.4
625	133.17	4.330	692.58	324.9	1713.5	0.008	587.8
		0.008	22.65	1.3	8.4	0.000	2.9
650	3.73	3.824	13.168	237.5	1519.5	0.418	453.5
		0.191	1.602	28.6	247.3	0.051	74.4
800	2.63	1.324	4.697	35.1	354.5	1.171	119.8
		0.400	2.004	15.0	212.9	0.500	73.4
1100	3.05	1.965	1.111	63.9	30.8	4.952	138.8
		0.436	0.405	23.3	16.4	1.807	72.6
1575	0.22	4.204	2.105	300.7	69.0	2.613	145.3
		0.773	1.000	142.7	48.3	1.241	103.1

Isotopic ratios have been multiplied by the factors indicated. Sample weights and irradiation constants (*J* values) are also indicated. Age uncertainties include only the error in $^{40}Ar/^{39}Ar$ and not the error in *J*.

Forward

Back

Table of Contents